Proceedings of Proceedings of the ASME 2023
International Mechanical Engineering Congress and Exposition
IMECE 2023
Oct 29 – Nov 2, 2023, New Orelans, LA, USA

IMECE2023-113518

PART 1: GYROSCOPIC CONTROL OF ROBOTIC SMART VEHICLES USING SO(3)

Jason Chen
The Cooper Union
New York, NY 10003

Eunkyu Kim
The Cooper Union
New York, NY 10003

Calder Leppitsch
The Cooper Union
New York, NY 10003

Benjamin Meiner
The Cooper Union
New York, NY 10003

Daniel Zaretsky
The Cooper Union
New York, NY 10003

Thorstein Ravneberg Rykkje
Western Norway University of Applied Sciences (HVL)
Bergen, Norway

Dirk M. Luchtenburg*
The Cooper Union
New York, NY 10003
Email: Dirk.Luchtenburg@cooper.edu

Thomas J. Impelluso
Western Norway University of Applied Sciences (HVL)
Bergen, Norway

ABSTRACT

In response to challenges faced in engineering education, this paper presents the Moving Frame Method (MFM) as an alternative to the existing pedagogies. This paper, and a companion paper, present the MFM for the analysis of rigid single-bodies, in the context of an international collaborative senior design project between two engineering schools: Cooper Union in New York, NY and The Western Norway University of Applied Sciences, in Bergen, Norway.

Students at Cooper Union analyzed the smart-vehicle as a single-body problem; a second team in Norway used the same method to model the problem as a multi-body. Both teams modeled the gyroscopic lift effect using the foundational theory of the MFM. This first paper presents the underlying theory of how the MFM uses the Special Orthogonal Group, SO(3), to model the problem of gyroscopic lift of a smart vehicle. It presents the underlying theory: motion of a reference frame in terms of the reference frame; and the various properties of SO(3) and its associated algebra as applied to a new, undergraduate approach to dynamics.

The paper presents how the modeling process led into a design which used two gyroscopes to pitch the vehicle, a four-wheeled car, while mitigating the yaw component. Next, it examines the model-generated estimates for torque generated and subsequent motion of the car. After analysis using the initial model, the Cooper Union Team pivoted in design approach before entering the rapid prototyping phase of the project. Then, it discusses the manufacturing process for the final version of the car and the construction of a test enclosure for ensuring safety by containing the heavy reaction wheel spinning at high speeds. Finally it describes the testing of the car, which involves measurement of angular impulse due to a braking event. The results from initial experiments on the prototype validate the model and confirm that the car can lift itself using the selected method.

*Address all correspondence to this author.

1 Introduction

1.1 Engineering education

The Chronicle of Higher Education has reported that nearly 1.3 million students have disappeared from American colleges during the Covid-19 pandemic, raising alarms that the enrollment emergency projected to arrive a few years from now is already here [4]. Campuses must now focus on way to retain and engage students; in fact, student engagement is now a priority across campuses worldwide.

Each academic discipline must find ways to retain and inspire students. This paper and its companion address this concern within the pillar of mechanical engineering. It does so by deploying a redevelopment of a discipline: rigid single and multi-body dynamics.

Dynamics is a gateway course to the mechanical engineering major. The traditional approach to this discipline deploys an understanding, mathematical notation, and associated algebra, that is founded on inertial frames and 2D motion. This limits the study of machines to two-dimensional problems. This lends an appearance of unrealistic solutions that obfuscates the theory of motion and confuses students.

However, in this contemporary age, mobile devices have onboard inertial firmware. We feel this may undermine attempts to inspire students.

In this project and its follow-on, we deployed a new mathematical approach to dynamics: the Moving Frame Method (MFM).

1.2 Moving Frame Method

Inertial reference frame are only approximations; and today's machines, with on-board inertial firmware, know their motion. The authors deployed modern mathematics [6] to redevelop the discipline of dynamics. This new approach uplifts the discipline from artificial planar problems (2D vector mathematics) to the study of 3D real world problems and inspires students.

The MFM places moving frames on every object [2] and relates them by exploiting Lie Group theory and its associated algebra, distilled to the simplicity of matrix multiplications. The MFM strictly adheres to moving reference frames (commensurate with our times) to develop the equations of motion. The MFM appears to manifest notational overload. However, once accustomed to it, students readily adapt and adopt the method. A suite of pedagogical interventions, developed by the guiding professor, facilitates learning.

The foundation of the MFM is presented in a lower division class and discussed and assessed in a related paper [7] Briefly, the author presented the method in 5000 pages of text documents. However, these text documents present single concepts on each page, and multiple repetitions of evolving figures; i.e., a final illustrative figure is not presented (from which, students must dig out all terms). Rather, figures are repeated many times on each e-page, as terms are added. Equations are colored and repeated. The result is that students readily "swipe" through the content and, with such distance, can focus on patterns, along with the theoretical development. Voiced PowerPoints with extensive animations are designed to excite students. Finally the pedagogical content is equipped with 3D physics-based animations that run on cell phones.[1]

The MFM has been used to model ROV motion [1], a 3D rotary pendulum [9], study friction [10], study gyroscopic wave energy converters [8], model a knuckle boom crane [3], and ship stability [5]. In this project, we apply it to a gyroscopic car lift, and, in the process, present further insight into how to empower engineering education.

1.3 Problem description

The project concerns the analysis and experimental validation of the gyroscopic lift of a smart vehicle. In a complete state, the vehicle would be able to autonomously traverse a typical human-sized set of stairs by sensing the position of ledges in front of it. It pitches its front wheels upwards into the air using gyroscopically generated torque until they reach over the top of the stair above. During the lifting time, it drives forward and places its upper wheels on the upper stair, at which point the gyroscope reverses its torque output to lift the rear wheels up while moving forward on the upper stair until it reaches a static state at the top of the stair.

2 Materials and methods

2.1 Moving frames and rotation matrices

In Fig. 1, a simplified model of a car with one gyroscope is shown. The figure also shows the definitions of the four reference frames that are used for kinematic analysis. In MFM, three orthonormal vectors and an origin make up a frame. A fixed frame $\mathbf{E}^{(0)}$ with origin O and orthonormal basis vectors $\mathbf{e}_1^{(0)}$, $\mathbf{e}_2^{(0)}$, $\mathbf{e}_3^{(0)}$ is attached to a fixed observer (lab or world frame). Similarly, moving frames are attached to all moving parts of the car: the first moving frame $\mathbf{E}^{(1)}$ is represented via orthonormal basis vectors $\mathbf{e}_1^{(1)}$, $\mathbf{e}_2^{(1)}$, $\mathbf{e}_3^{(1)}$ with its origin fixed at the center of mass of the vehicle and moves with with the chassis of the vehicle. Moving frame $\mathbf{E}^{(2)}$ is attached to a vertically spinning axis, and frame $\mathbf{E}^{(3)}$ is attached to the spinning disk. Since the disk is heavy compared to the other components of the vehicle we only consider the inertia of the disk in our model. Therefore, frame $\mathbf{E}^{(3)}$ is also referred to as the body frame.

There are two rotations that we need consider for this problem. The first rotation is from frame $\mathbf{E}^{(1)}$ to $\mathbf{E}^{(2)}$ around the $\mathbf{e}_3^{(1)}$ direction with angle ψ, and the second rotation is from $\mathbf{E}^{(2)}$ to $\mathbf{E}^{(3)}$ around the $\mathbf{e}_2^{(2)}$ direction with angle ϕ. We note that the

[1] See the following webpage: https://home.hvl.no/ansatte/jim/MAS112/

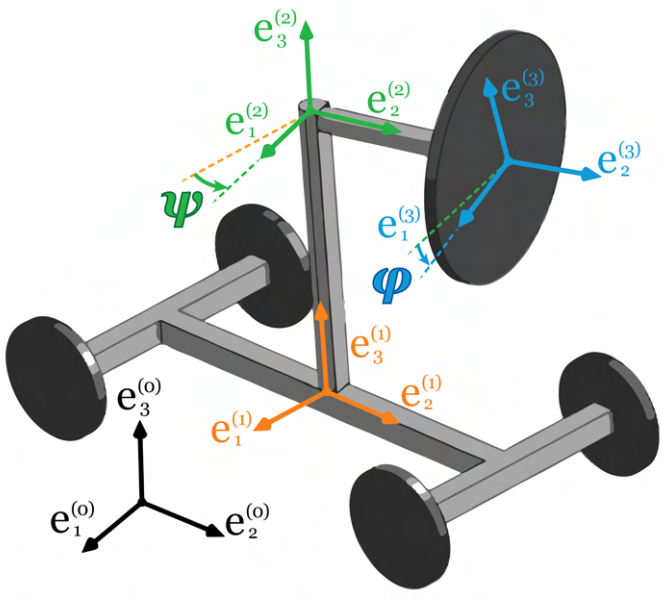

FIGURE 1. Vehicle with one gyroscope.

moving frames are time dependent and are related by rotation matrices. For example, the relationship between $\mathbf{E}^{(1)}$ and $\mathbf{E}^{(2)}$ is as follows

$$\left[\mathbf{e}_1^{(2)}\ \mathbf{e}_2^{(2)}\ \mathbf{e}_3^{(2)}\right](t) = \left[\mathbf{e}_1^{(1)}\ \mathbf{e}_2^{(1)}\ \mathbf{e}_3^{(1)}\right](t) \begin{bmatrix} \cos(\psi(t)) & -\sin\psi(t)) & 0 \\ \sin(\psi(t)) & \cos\psi(t)) & 0 \\ 0 & 0 & 1 \end{bmatrix}$$

This relationship can be written using a compact notation as in [9]

$$\mathbf{E}^{(2)} = \mathbf{E}^{(1)}\mathbf{R}^{(1,2)}. \tag{1}$$

Similarly, frame $\mathbf{E}^{(2)}$ and $\mathbf{E}^{(3)}$ are related by

$$\mathbf{E}^{(3)} = \mathbf{E}^{(2)}\mathbf{R}^{(2,3)}, \tag{2}$$

where $\mathbf{R}^{(2,3)}$ is the rotation matrix around the 2-axis, see the Appendix. Combining the above relationships, we have

$$\mathbf{E}^{(3)} = \mathbf{E}^{(2)}\mathbf{R}^{(2,3)} = \mathbf{E}^{(1)}\mathbf{R}^{(1,2)}\mathbf{R}^{(2,3)} = \mathbf{E}^{(1)}\mathbf{R}^{(1,3)}. \tag{3}$$

In the following, we assume that the vehicle direction is fixed and aligned with the inertial frame, i.e. $\mathbf{E}^{(1)} = \mathbf{E}^{(0)}$.

2.2 Moving frames and angular velocities

In MFM the rate of change of a frame, i.e. the angular velocities, are expressed in the moving frame itself. This leads an elegant representation in the form of a skew-symmetric matrix.As an example, we how the time rate of change of frame $\mathbf{E}^{(3)}$ is obtained. We use the dot notation to represent the time derivative with respect to the fixed frame ($d/dt(\ ) = \dot{(\ )}$). The relationship between frame $\mathbf{E}^{(3)}$ and the fixed frame $\mathbf{E}^{(0)}$ is given by

$$\mathbf{E}^{(3)} = \mathbf{E}^{(0)}\mathbf{R}^{(0,3)}. \tag{4}$$

Taking the time derivative with respect to the fixed frame, we obtain

$$\dot{\mathbf{E}}^{(3)} = \mathbf{E}^{(0)}\dot{\mathbf{R}}^{(0,3)} = \mathbf{E}^{(3)}\mathbf{R}^{(3,0)}\dot{\mathbf{R}}^{(0,3)}, \tag{5}$$

and since rotation matrices are orthogonal $\mathbf{R}^{(3,0)} = (\mathbf{R}^{(0,3)})^T$, we can write

$$\dot{\mathbf{E}}^{(3)} = \mathbf{E}^{(3)}(\mathbf{R}^{(0,3)})^T\dot{\mathbf{R}}^{(0,3)} \tag{6}$$

The product of the transpose of a rotation matrix and the time derivative of a rotation matrix is a skew-symmetric matrix composed of the components of the angular velocity [9]:

$$\dot{\mathbf{E}}^{(3)} = \mathbf{E}^{(3)}\,\tilde{\omega}_{3/0}^{(3,3)} \tag{7}$$

where

$$\omega_{(3/0)}^{(3)} = \begin{pmatrix} \omega_1^{(3)} \\ \omega_2^{(3)} \\ \omega_3^{(3)} \end{pmatrix}$$

is the angular velocity of the body frame with respect to the inertial frame *expressed in the body frame* $\mathbf{E}^{(3)}$ and

$$\tilde{\omega}_{3/0}^{(3,3)} = \begin{pmatrix} 0 & -\omega_3^{(3)} & \omega_2^{(3)} \\ \omega_3^{(3)} & 0 & -\omega_1^{(3)} \\ -\omega_2^{(3)} & \omega_1^{(3)} & 0 \end{pmatrix} \tag{8}$$

is the corresponding skew-symmetric matrix.

2.3 3D dynamics

This section demonstrates how to use the MFM along with Euler's 2nd Law to derive the governing equation of motion of rotating spinning disks.

Euler's second law describes the relationship between a system's change angular momentum, $\dot{\mathbf{H}}_c$, and the net external moment $\mathbf{M}_c$ on the system where C is the center of mass

$$\dot{\mathbf{H}}_c = \mathbf{M}_c \tag{9}$$

The gyroscope is modelled as a disk which has a diagonal mass moment of inertia matrix, $J_c^{(2,2)}$, due to symmetry. We choose to express the angular momentum in $\mathbf{E}^{(2)}$. In general, it is recommended that angular momentum is expressed in the body frame as the mass moment of inertia matrix is constant in that frame. However, in this problem, due to axial symmetry, the mass moment of inertia matrix is the same in frame $\mathbf{E}^{(2)}$.

Expressing the angular momentum with respect to the center of mass, $\mathbf{H}_c$, in frame 2, $\mathbf{E}^{(2)}$, we obtain

$$\mathbf{H}_c = \mathbf{E}^{(2)} J_c^{(2,2)} \omega_3^{(2)}. \tag{10}$$

Next, we calculate the time derivative using the chain rule

$$\dot{\mathbf{H}}_c = \dot{\mathbf{E}}^{(2)} J_c^{(2,2)} \omega_3^{(2)} + \mathbf{E}^{(2)} J_c^{(2,2)} \dot{\omega}_3^{(2)}$$

Using the fact that $\dot{\mathbf{E}}^{(2)} = \mathbf{E}^{(2)} \tilde{\omega}_2^{(2,2)}$, we obtain

$$\dot{\mathbf{H}}_c = \mathbf{E}^{(2)} \left(\tilde{\omega}_2^{(2,2)} J_c^{(2,2)} \omega_3^{(2)} + J_c^{(2,2)} \dot{\omega}_3^{(2)} \right) = \mathbf{E}^{(2)} \dot{\mathbf{H}}_c^{(2)}, \tag{11}$$

which is an expression for the time derivative of angular momentum expressed in $\mathbf{E}^{(2)}$.

For one single gimbal gyroscope with spin angular velocity $\dot{\psi}$ and gimbal angular velocity $\dot{\phi}$, the rate of change angular momentum components are

$$\dot{\mathbf{H}}_c^{(2)} = \begin{bmatrix} -J_2 \dot{\phi} \dot{\psi} \\ J_2 \ddot{\phi} \\ J_1 \ddot{\psi} \end{bmatrix} \tag{12}$$

2.3.1 Car with two gyroscopes Next we consider two gimbal gyroscopes, and denote the angles of the first gyroscope by ϕ_A and ψ_A, and the angles of the second gyroscope by ϕ_B and ψ_B, thus we obtain

$$\dot{\mathbf{H}}_{c,total}^{(2)} = \begin{bmatrix} J_2 \left(-\dot{\phi}_A \dot{\psi}_A - \dot{\phi}_B \dot{\psi}_B \right) \\ J_2 \left(\ddot{\phi}_A - \ddot{\phi}_B \right) \\ J_1 \left(\ddot{\psi}_A - \ddot{\psi}_B \right) \end{bmatrix} \tag{13}$$

Assuming perfectly synced motion of gyroscope A and gyroscope B with opposite angles and rates out, the equation reduces to

$$\dot{\mathbf{H}}_{c,total,sync}^{(2)} = \begin{bmatrix} -2J_2 \dot{\phi} \dot{\psi} \\ 0 \\ 0 \end{bmatrix}. \tag{14}$$

In the vehicle chassis frame, $\mathbf{E}^{(1)}$, the rate of change angular momentum components are

$$\dot{\mathbf{H}}_{c,total,sync}^{(1)} = \begin{bmatrix} -J_2 \cdot \left(2\mathrm{s}(\psi) \ddot{\phi} + 2\mathrm{c}(\psi) \dot{\phi} \dot{\psi} \right) \\ 0 \\ 0 \end{bmatrix}, \tag{15}$$

where sin and cos are abbreviated by s and c respectively. Assuming that the disks spin with constant rotational velocity, the required torque or moment is given by Euler's second law, $\mathbf{M}_c = \dot{\mathbf{H}}_c$,

$$\mathbf{M}_c = \mathbf{E}^{(1)} \begin{pmatrix} -2J_2 c(\psi) \dot{\phi} \dot{\psi} \\ 0 \\ 0 \end{pmatrix} \tag{16}$$

By Newton's third law, the torque on the vehicle is

$$\mathbf{M}_{vehicle} = -\mathbf{M}_c,$$

and *we conclude that a combination of two counter-rotating gimbals can be used to lift a vehicle around its pitch axis* $\mathbf{e}_1^{(1)}$, see Fig. 1.

Figure 2 displays the moment applied to the car through the use of two perfectly synced gyroscopes spinning at a constant velocity.

2.3.2 Dual-gyro approach – Design calculations To determine if the control moment gyroscope (CMG) approach will produce successful results in this application, it is necessary to calculate the required gyroscope size and speed to lift a small vehicle. The result of the calculation provides a justification as to whether the approach is a viable solution to the problem addressed in this paper.

The proposed case uses two gyroscopes which are in perfect sync to cancel undesirable moments. Only rotation in the pitch axis is required; there should ideally be no rotation in the yaw or roll axes. Using two gyroscopes means that a pitch rotation can be generated while the two gyroscopes rotate in opposite directions cancelling out any yaw or roll moments. Therefore the

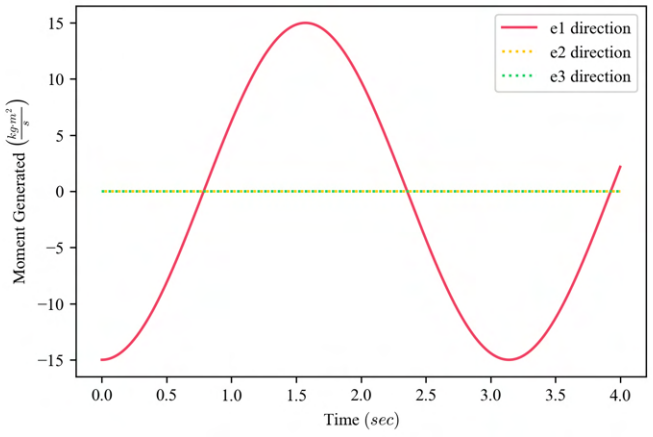

FIGURE 2. Moment applied to car in vehicle frame $\mathbf{E}^{(1)}$

CMG approach requires the vehicle to have two gyroscopes and gimbals.

To begin calculations, placeholder values are chosen to represent the weight and size of the vehicle. The vehicle includes the frame structure, motors to drive the wheels, and a battery pack. The two gyroscopes each require a gimbal structure, a spin axis motor, and a secondary axis motor. Taking the mass of the vehicle frame and parts to be two kilograms with a frame length (axle to axle) of 30cm, the problem can be approached as a rigid body rotating about a hinge point at the rear wheel axis. The moments acting on the rigid body are the gyroscopically generated moment and the torque due to gravity acting on the mass of the vehicle. The line through the rear wheel axis and the center of mass is taken to be 20 degrees inclined vertically from the horizontal.

The most immediate limitation of the governing equations with respect to reality is the velocity of both the reaction wheel and the gimbal. The velocity of the reaction wheel is limited by the capability of the motors used and the safety of rotating a potentially unbalanced mass at high speed. An additional constraint is placed on the velocity of the gimbal due to the fact that a high rotation speed decreases the exposure time of the vehicle to any meaningful torque as seen in Figure 2. The moment generated peaks when the gimbal axis is orthogonal to the axis of rotation, then falls and reverses.

The above factors place an extreme upper limit of 10,000 RPM on the spin axis velocity. The limit is extreme because speeds of this magnitude are dangerous and would require strengthening the design of the gimbal and frame structure which increase the total weight of the vehicle and reduce the effectiveness of the generated moment. The limit placed on the gimbal axis velocity is approximately 4 radians per second or 38.2 RPM to allow for 0.5 seconds of exposure to at least 50 percent of the maximum moment generation. This provides the vehicle a small window of time to drive towards the stair while the front wheels are lifted into the air.

To determine the size of gyroscopes required to lift the vehicle, a numerical integration routine is used to calculate the motion of the car when subjected to one 180 degree rotation of the synced gyroscope-gimbal systems. Since the weight of the gyroscopes has an effect on the total weight of the car, the optimization of the moment of inertia of the disk is of the utmost importance. In the ideal case, the gyroscope is made of solid tungsten with density 19.30 grams per cubic centimeter and the mass is distributed in the shape of a hollow cylinder with an inner radius of 0.6 times the outer radius. Using these values, there is a functional relationship between the radius and thickness of gyroscope that can lift the car. Two possible values are are displayed in Table 1.

Thickness (cm)	Outer Radius (cm)	Inner Radius (cm)
1.0	3.9	2.34
2.5	3.3	1.98

TABLE 1. Optimal Gyroscope Parameters.

A more realistic set of values for the operation of the synced dual-gyroscope setup is a gyroscope speed of 2000 RPM and a gimbal speed of 20 RPM. If the gyroscope is made of solid brass with density 8.73 grams per cubic centimeter and has a inner to outer radius ratio of 0.5, a different set of possible values are available. Brass is chosen because it is an affordable material and it is easy to machine. The requirements for this setup can be seen in Table 2

While this design seems achievable, it will likely require extensive optimization as the outer radii in the above table will result in gimbal and motor structures that are too large to mount onto a 2kg frame. Increasing the size and weight of the frame will also mean redesigning the gyroscope parameters to ensure that the car will lift. Additionally, the values shown in the table are the minimum required to achieve a lift. A higher than one factor of safety will be required to ensure consistent performance and account for energy losses due to unmodeled effects. Due to these facts, an alternative design is proposed which will allow for more straightforward manufacturing and control.

2.3.3 Reaction wheel approach An alternative design setup involves a reaction wheel spinning about the axis perpendicular to the ground. It involves applying a braking mechanism on the reaction wheel as to alter the spin velocity $\dot{\phi}$. The

Thickness (cm)	Outer Radius (cm)	Inner Radius (cm)
2.5	8.0	4.0
5	7.6	3.8

TABLE 2. Realistic Gyroscope Parameters

inspiration of this idea came from an existing device called the Cubli: a small cube that has three reaction wheels giving it complete control over its motion and angle.[2] In theory, there are two ways to use reaction wheels, deceleration mode or acceleration mode. Either of these will produce moments, but to produce enough moment to make something jump into the air, it is necessary to decelerate the reaction wheel using a brake. The motor alone cannot accelerate or decelerate the reaction wheel with enough magnitude for lift. However, stabilization of the vehicle once it is in an inverted pendulum position is achievable via controlled acceleration using solely actuation of the spin axis motor.

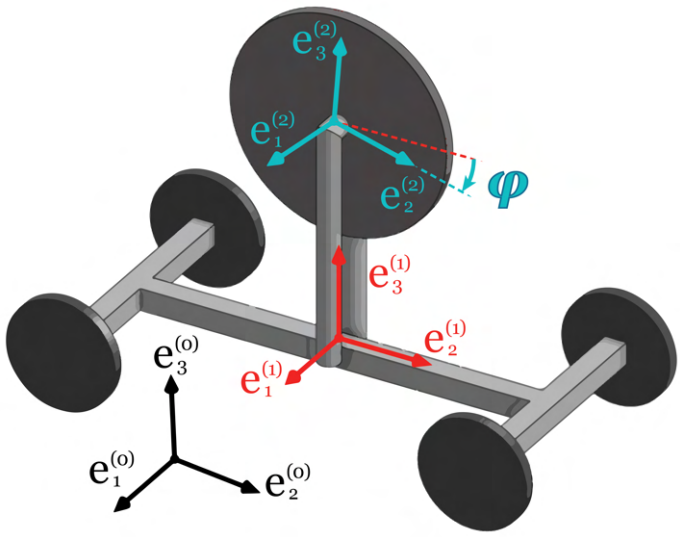

FIGURE 3. Vehicle with a reaction wheel.

As for the previous model, we use a simplified version seen in Figure 3 with $\mathbf{E}^{(1)}$ coinciding with the orientation of the vehicle. $\mathbf{E}^{(2)}$ or the body frame is attached to the reaction wheel, rotating with the reaction wheel spin angle ϕ. Using Euler's 2nd law as before, we arrive at an expression for the angular momentum in $\mathbf{E}^{(2)}$.

$$H_C^{(2)} = \begin{bmatrix} J_2\dot{\phi} \\ 0 \\ 0 \end{bmatrix} \tag{17}$$

Therefore, the time derivative of angular momentum is:

$$\dot{H}_C^{(2)} = \dot{H}_C^{(1)} = \begin{bmatrix} J_2\ddot{\phi} \\ 0 \\ 0 \end{bmatrix} \tag{18}$$

Hence, if a braking mechanism is applied to the reaction wheel, the net moment produced on the vehicle is the negative of equation (18)

$$\mathbf{M}_{vehicle} = \mathbf{E}^{(1)} \begin{pmatrix} -J_2\ddot{\phi} \\ 0 \\ 0 \end{pmatrix} \tag{19}$$

The process of determining whether the reaction wheel-based vehicle will function is similar to the CMG viability calculation. The moment generated by this apparatus is modeled as a step function, where it is assumed that the moment caused by braking is from a constant force over a period of time. Once again, the motion of the vehicle is modeled as a rigid body rotating about a hinge point due to an applied moment opposed by the torque due to gravity. The lift time is calculated using the same numerical integration method as for the CMG. The output of the simulation is a calculation of the required initial RPM, assuming constant deceleration and zero final velocity. In reality, the braking force will not be constant during the lifting period, but the calculation gives ballpark values with which to compare experimental results. In the script used for the calculation, the relationship of interest was the initial RPM with respect to the applied braking force. Table 3 shows a couple selected values.

The values used for the mass of the vehicle, the position of the center of mass, and the moment of inertia of objects all come from the dimensions and materials of the actual prototype and were measured from the physical model or CAD software.

3 Design and manufacturing

The first step in designing a car that will climb a stair is selecting the optimal overall geometry for the car. The most obvious limitations are that the car needs to be shorter than the length of the stair while also being somewhat longer than the height of the stair. These requirements are necessary to allow the car's front wheels to reach the stair above it. Typical stairs have a stair height (or rise) 3-5 inches less than the length (also called the

[2] Cubli - Institute for Dynamic Systems and Control

Brake Force (N)	Initial Speed (RPM)	Time to Lift (sec)
40	1685.2	0.147
100	2178.1	0.076

TABLE 3. Reaction Wheel Simulation Results

tread) making this possible. Another important aspect of the car design is that the front wheels of the car must be able to reach around the lip and over the top of the stair ahead of it without the structure of the car colliding against the surface and losing the ability to move. The weight distribution of the car is also an important factor. The car needs to be able to rotate in both directions. This means keeping the center of mass around the center of the car makes the most sense. Additionally, the center of mass should not be excessively high. If the car is top heavy, it risks tipping over when pitching upwards and creates further challenges in controlling its angle.

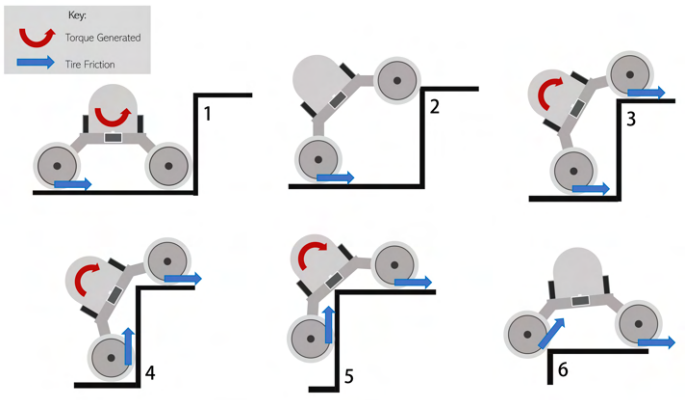

FIGURE 4. Process of car climbing a stair.

Figure 4 shows how the car will maneuver up a set of stairs. It begins with the car flat on a stair. Inducing a moment lifts the car vertically, where it can be controlled and precisely lowered onto the stair above it. Then it induces a moment opposite the previous one to lift the car the other way where it can drive forward and rest on the stair. This process repeats as it traverses the stairs.

3.1 Material and manufacturing options

When designing the car, several materials were considered for prototyping as well as more optimized models. The main priority for material selection is strength to weight ratio as well as simplicity of manufacturing. The costs of different materials and availability were also considered when prototyping to reduce project costs and keep the project on schedule. Several fabrication methods were explored such as 3D printing, laser cutting, and machining on a lathe and mill. Tolerance of parts and the precision afforded by each machine had to be considered for each component to minimize manufacturing time and complexity.

The prototype frame is manufactured using 3D-printed Polylactic acid (PLA) and Acrylonitrile styrene acrylate (ASA) as well as laser cut cast acrylic sheets. These components were bolted together using M3 steel screws of various lengths and nuts. For some applications, brass threaded inserts were placed into the 3D-printed parts to interface with the screws. These were installed by pressing with a soldering iron to temporarily melt the surrounding plastic as it is seated into the plastic.

Components that are subject to the highest mechanical stress were constructed using PLA since it can form strong and complex structures, infill density can be varied based on anticipated stress distribution, and it can be easily modified with hand tools. Acrylic sheets were used to connect the components of the frame together since it is lightweight and quickly cut. For all of the high-speed components, including the reaction wheel and associated mounting, aluminum was used and it was hand machined on the lathe and mill. Aluminum was the material of choice for the high-speed components because of its ability to handle high stress during reaction wheel acceleration and braking. The aluminum components were machined precisely to minimize vibration due to unbalanced mass.

3.2 Prototyping

3.2.1 Initial prototype Initially the entire chassis was modeled to be a one piece monocoque design. The car consisted of an arch shaped 3D printed frame. Then two acrylic panels fit on the sides which housed the smaller motors for driving the wheels. This design was chosen because it provided a very simple construction method: the entire frame would be printed out in one piece. This would make construction simple as only cleanup on a 3d print would be required. Immediate issues were encountered when printing it. Calculations pointed out that a larger reaction wheels was required to generate adequate pitch. As a result, the frame was lengthened to accommodate the larger wheel. This resulted in the frame not fitting within the print bed of even the largest 3D printer available in the school. Printing with the ends of the frame cut off resulted in very poor stiffness when the car was supported by wheels because the motors were only attached to free floating acrylic plates. There would be a significant wobble side to side from any forces.

An additional problem was the lack of clearance for installing the reaction wheel. Since the frame was one piece, the reaction wheel had to be slotted into the frame and then the axial components pushed through. With the very small tolerances, it

was difficult and time consuming to remove and install the reaction wheel assembly during testing. The most problematic issue was the lack of full support for the heavy reaction wheel. In this design, the reaction wheel is only supported by the motor. This creates a significant cantilever stress on the motor which could damage it or reduce performance. The pitfalls of this prototype gave insight on how to improve the next version.

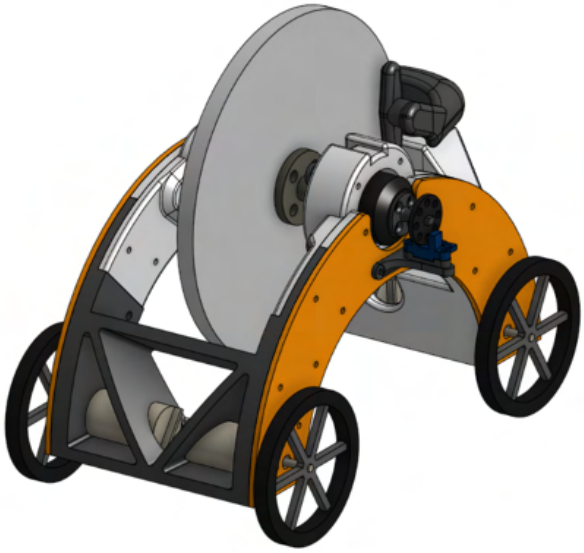

FIGURE 5. Final prototype CAD assembly rendering.

3.2.2 Final prototype The final prototype takes a radically different approach by creating six smaller frame pieces lapped together and connected by two acrylic side panels. The new smaller pieces greatly improve the serviceability and promotes modular design. Additionally, this design improved the prototyping process because team members could be assigned to design one section which is far more streamlined than having multiple people working on one chassis piece.

The entire reaction wheel assembly can be accessed by removing one acrylic side panel and one frame section. Additionally, the frame section on the port side has an integrated a cutout for the wires that bring power to the central motor which spins the reaction wheel. These wires are routed to outside the frame to prevent wires getting caught in the spinning parts. The same frame section also integrated the bolt pattern for a bracket that came with the the motor which removed the need to fabricate a custom mount. The starboard frame section now has a hole

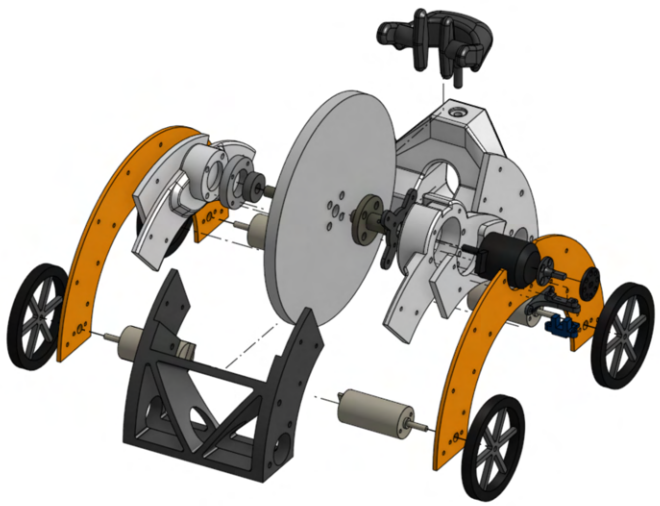

FIGURE 6. Exploded view of final prototype CAD.

which fits a ball bearing and supports the other side of the reaction wheel assembly to mitigate the cantilever force on the motor axle.

There is a front truss spanning the two acrylic side panels. Significant weight reduction in the form of triangular holes was implemented to reduce the weight while retaining similar strength. A circular hole runs through the entire truss horizontally which provides great support and stiffness to the wheel motors. The rear truss is of a similar design but without the triangular holes because it houses the brake caliper and additional factor of safety was desired. It uses an arch design which distributes the loads of braking effectively into the rest of the chassis. Servicability was also considered. The arch shape also allows an Allen wrench to fit inside to tighten the caliper. An additional 8 mm hole was made on the bottom of the truss to allow quick tightening with a screwdriver. Also of note, the rear truss uses progressive infill density. The top section of the rear truss was printed with 100% infill because significant pressure would be put onto the plastic when the caliper is bolted in and when braking is applied.

All of the frame pieces are held together using an system of lap joints, brass inserts, acrylic pieces, and M3 hardware. The port and starboard frame pieces are lapped with the two trusses. Two bolts run through each lap joint and the acrylic side plates. This adds additional strength to the frame and prevents separation. This system proved to be very strong and no deformation of the chassis was observed. The frame held up to a rotating reaction wheel of 8,000 rpm and withstood braking forces with no issues.

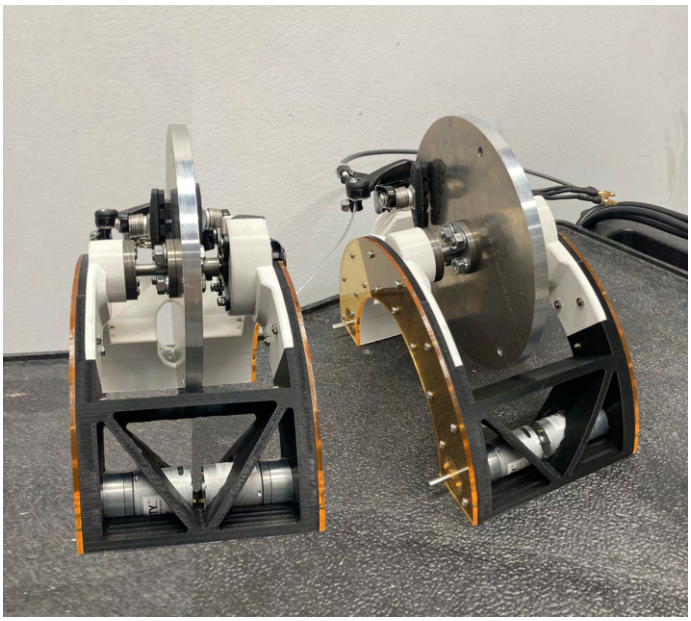

FIGURE 7. Final prototype fully assembled.

3.3 Motors

Two different types of motors were chosen for the design of the car. The motors for the wheels are 124 rpm brushed DC motors. These are simple to control and provide the necessary speed and torque for moving the car. The reaction wheel motor is a brush-less DC motor (Emax GT2815) rated for 12V. This motor is designed for drones and can reach the high RPM needed to generate enough angular momentum. The motor controller used was a Hobbywing Skywalker rated for 12V 80A. This motor controller is designed for use with remote controls however, an Arduino was used to send commands to the controller to set the speed.

3.4 reaction wheel and brake

The reaction wheel is constructed of a single aluminum disk. It was determined that reducing weight near the center of the wheel to get a better rotational inertia to weight ratio failed to produce worthwhile benefits. As such the disk was kept whole to simplify manufacturing. The hole bored in the aluminum disk did not match the shaft diameter of the motor or bearing. To remedy the issue, two adapter flanges were machined from mild steel. The flanges are bolted into the reaction wheel with 4 equidistant bolts. One flange fits over the motor shaft and is secured using a set screw. The other flange slots into the 5mm bearing.

The brake is a standard bicycle caliper rim brake. Due to the small diameter of the reaction wheel, the translational velocity at the brake was calculated to be similar to what would be experienced on a bicycle. The brake is cable actuated and a servo will be controlling the tension on the cable. Testing showed that the brake and reaction wheel system worked without issues.

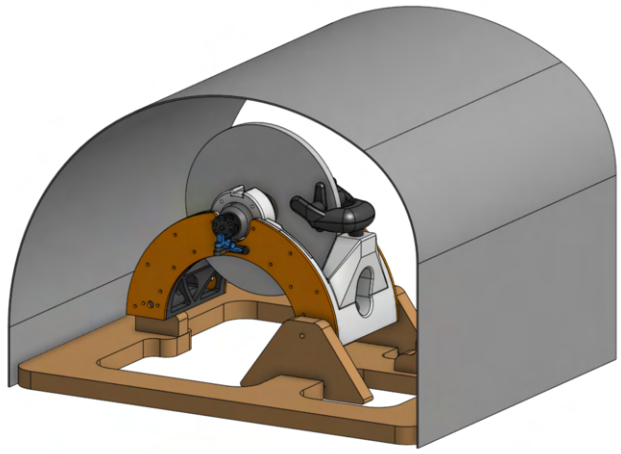

FIGURE 8. Safety cage CAD assembly rendering.

3.5 Test Stand design and construction

The test stand was designed with the safety of the experimenter in mind. If the reaction wheel spinning at high RPM were to come loose, it is possible for it to hit something and fly at a high velocity outwards from the vehicle. If this were to happen and there was no shielding it would be extremely dangerous for anybody in the vicinity. The possibility of such an event occurring is not negligible. If one of the rotating parts such as the bearing or the motor itself heats up drastically, it could melt the surrounding PLA and subsequently the entire vehicle would have a rapid unplanned disassembly.

In order to avoid catastrophe, the test stand was designed to withstand impact of a large magnitude. The test stand was constructed using wood, steel, aluminum and polycarbonate. The bottom of the stand was made from wood, with a mounting bracket for the shafts of the back motors. There were also wooden stoppers with polyethylene foam mounted to prevent damage to the frame from an impact when it swung back from the torque. Attached to this wooden base, was a cover to prevent any impact during possible failure. It was made from an aluminum sheet curved to match the arc of the car during movement. It had sideplates one made from steel an one made from clear polycarbonate to allow for viewing of the car during testing. Several holes were drilled into the polycarbone panel to route cables and wires for the sensors, electronics, and brake cable. This cover was screwed into the wooden baseplate.

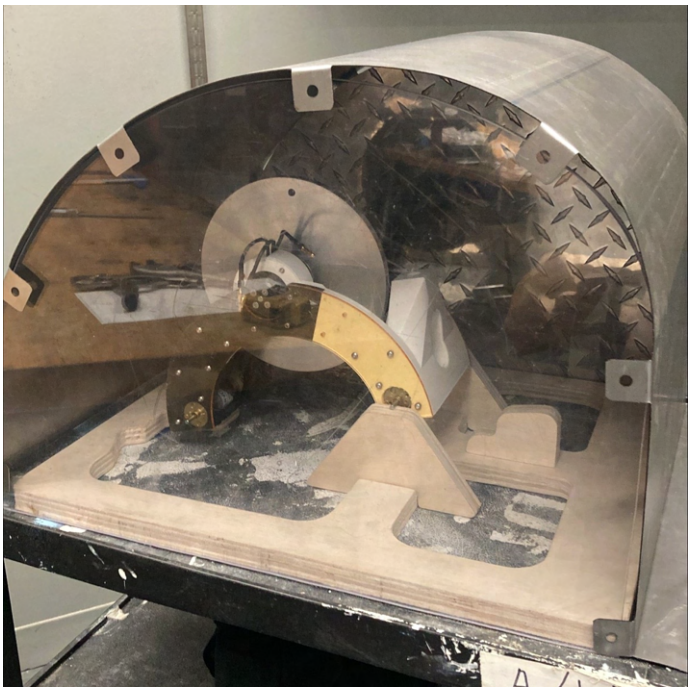

FIGURE 9. Safety cage during construction process.

4 Electronics and controls

To get data of the movement and abilities of the car, several sensors are incorporated into the test stand and car. The accelerometer and the strain gauge, which sample at a slower rate, are wired to one Arduino. The laser sensor and encoder is used to measure rotational speed and is wired to its own dedicated Arduino recording at a faster sampling rate.

4.1 Accelerometer

To get accurate data about the angular position and speed of the car, the MPU6050 3-axis gyroscope and 3-axis accelerometer module was used. This sensor connects to the Arduino using the I2C protocol. The sensor only outputs rotational acceleration and rotational velocity data. To obtain the angle rotated, Jeff Rowberg's MPU6050 library was used.[3]

4.2 Load Cell

The 10 kg load cell with HX711 amplifier was included to measure the force over time when the brake is applied to the reaction wheel. The direction of the reaction wheel is reversed such that breaking will result in the force going downwards (opposite of lift). The HX711 amplifier by default has a sample rate of 10 hz as listed on the data-sheet. The datasheet showed that there is an alternative higher sampling rate if pin 15 of the HX711 is set to high. A jumper was soldered to pull pin 15 to the VCC of 5V. The strain gauge was now measuring at a rate of 80 hz which worked better for measuring braking action over a short time span.

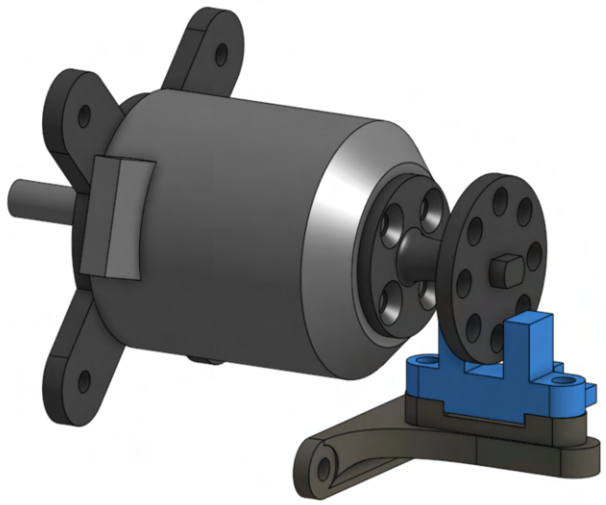

FIGURE 10. Rotational speed measurement CAD assembly

4.3 Rotational speed sensor

Another sensor included in the car was an IR LM393 rotational speed sensor. The rotation speed sensor sends an IR signal on one end and receives the signal on the other. A 3D printed encoder disk is placed between the IR signal and receiver and attached to the motor. The rate at which the receiver receives IR signals is used to calculate the speed of the motor and reaction wheel assembly. This provides a convenient method to log the speed of the reaction wheel during testing. The rotational speed sensor was connected to a separate Arduino because of the very fast sample rate needed to read the data pulses.

4.4 Motor control

The reaction wheel motor is connected to a separate Arduino from the sensors. This is because isolation from the other instruments was wanted. Power could be killed to both the Arduino and the motor if they needed to be stopped.

[3] Jeff Rowberg - Github

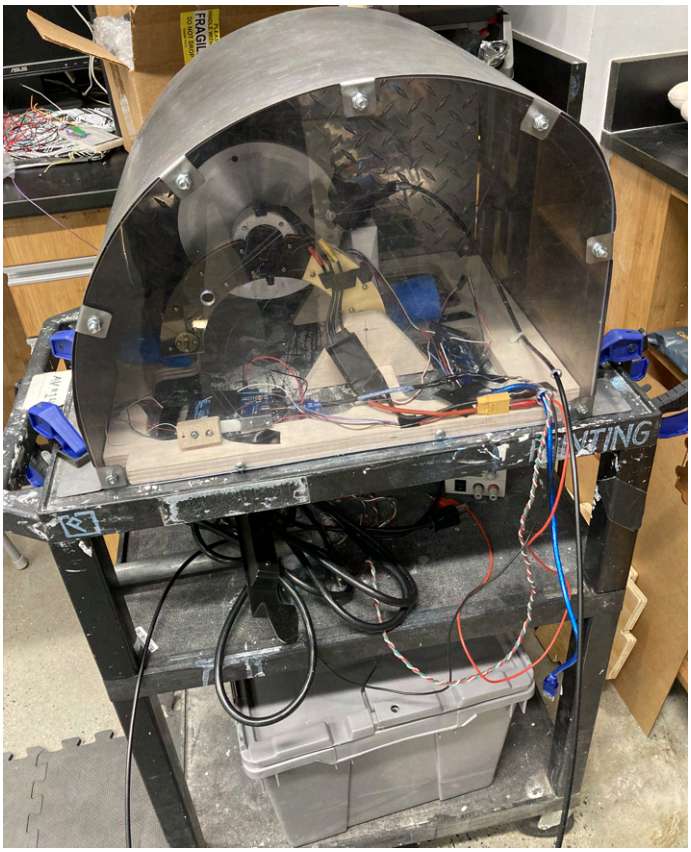

FIGURE 11. Test stand fully assembled and all instrumentation in place.

5 Experimentation

The primary goal of testing the prototype is to determine how accurately the model represents the system. A secondary goal of testing is to determine whether the design of the reaction wheel is sufficient to lift the car. The first goal is accomplished through a static test to measure the torque generated on the car frame by braking the reaction wheel. The frame is pinned at one of the wheel axes while the other remains free. Under the free wheel is places a load cell calibrated to read zero when the car is only under the force of gravity. Any load in excess of gravitational equilibrium is measured by the load cell.

The reaction wheel is spun counterclockwise as seen in Figure 9. When the brake is actuated, the force on the brake from the friction of the disk is transmitted through the frame to the free end supported by the load cell. The angular impulse generated by the braking event is measured in two ways. The first way is using the load cell force measurements to get torque around the pinned connection and integrating over time. The second way is using an encoder attached to the disk which measures the angular velocity. The change in angular velocity of the disk multiplied by its moment of inertia will result in the angular impulse. The testing procedure focuses on making the experiment simple to setup and producing reliable data. Data recording is automated by the use of electronic sensors and micro-controllers to remove any sources of human error.

5.1 Setup

The majority of the work needed to run the experiment is in the setup phase. Initially the wooden frame which acts as a base for the safety cage construction is placed onto a stable cart. Subsequently, the entire vehicle is attached to the wooden frame by inserting the axles of the wheel motors on one side through a hole, creating a pinned connection. The steel sheet-metal cover and polycarbonate window are lowered into place, bolted together, and screwed into the wooden frame. The steel edges of the safety cage that extend horizontally are used as a location to attach C-clamps which securely fix the entire assembly to the cart. All of the measurement devices have their corresponding Arduinos flashed with the required firmware so they are ready to record data and their USB cables are routed through a hole in the side of the polycarbonate window. The USB cables are connected to a laptop where the Arduino serial monitor logs data throughout the experiment and is saved for post-processing.

The load cell is calibrated by clamping one end to a table with a C-clamp, then placing a known mass onto it and recording the value output by the program reading the data from the load cell. This value is used to find constant of proportionality that relates voltage to the grams of the known mass, which is used in the Arduino code to output grams instead of voltage. The load cell is then installed onto the wooden test stand using a screw.

5.2 Data Collection

The test structure for data collection involved the selection of three different motor controller settings which each correspond to a certain top speed based on the number of amps drawn by the motor controller. For each of the motor controller settings, three trials were run to have a sampling of data points. Each trial begins by running a startup procedure for the motor and reaction wheel subassembly. The spinning subassembly eventually reaches terminal velocity, at which point in time the motor is shut off and the brake is actuated by hand using the brake lever until the subassembly stops spinning. After each test the data log is saved into an excel file.

The second goal of testing the prototype, to see if the reaction wheel causes the car to lift, required a minor change in the experiment setup. The polarity of the motor is switched to cause the rotating subassembly to spin in the opposite direction as the previous test, or clockwise in Figure 9. When the brake is applied, the torque that would have been measured by the load cell is used to rotate the entire vehicle frame clockwise over the pinned set of axles. This movement is fairly violent, which

required foam padding to be installed on the wooden support blocks that stop the vehicle and reaction wheel from colliding with the safety cage.

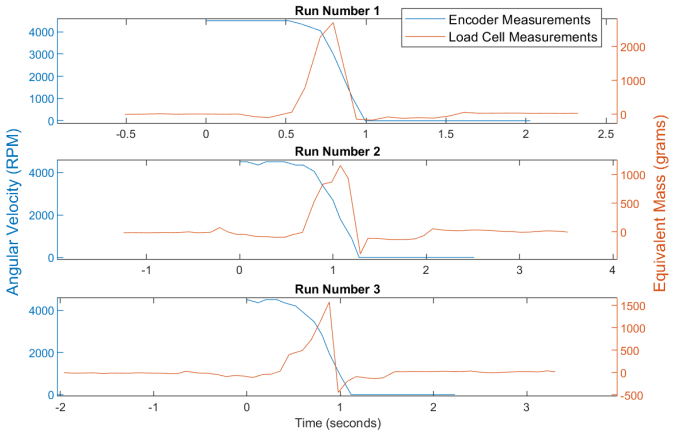

FIGURE 12. Raw test data for motor controller setting 1100.

5.3 Results

The experimentation process generated results that addressed both initial goals. The second goal, to lift the car dynamically, was accomplished relatively quickly as seen in Figure 13. It was found that a speed in the range of three to four thousand rotations per minute was able to fully bring the center of mass over the rear axle for a range of brake actuation strengths. This does not necessarily align with model results as there is no way currently to measure the brake actuation force, which is an important variable to determine the time variation of change in momentum. The MATLAB model used to simulate the movement of the car under experimental conditions found that the required starting speed varied widely depending on the force with which the brake is actuated, a trend which was corroborated by informal observations during the dynamic lift event tests.

The first goal, to determine model accuracy, was accomplished using the static test data, a sample of which can be seen in Figure 12. By comparing the angular impulse measured through two different methods, it seems possible that there are some unmodeled physics. Examining the results, seen in Table 4, it is clear that the angular impulse measured by the load cell is consistently lower than the encoder measurement.

To understand why there might be a difference, consider that both values are estimates of the true value. As stated previously, the encoder impulse assumes that all the deceleration of the reaction wheel from peak velocity to zero velocity is turned into torque applied to the load cell.

Motor Controller Setting	Peak Speed (RPM)	Load Cell Angular Impulse	Encoder Angular Impulse
1075	2262	0.735	0.592
1075	3600	0.827	0.943
1075	3450	0.582	0.903
1100	4500	1.305	1.178
1100	4500	0.875	1.178
1100	4500	0.915	1.178
1110	5100	1.077	1.335
1110	5100	0.902	1.335
1110	5100	0.986	1.335

TABLE 4. Test Results for Angular Impulse Measurement

A few inaccuracies in the model might reduce the amount of energy transmitted to the load cell. First, there is heat generated by friction between the brake and the reaction wheel. Second, the effect of the vehicle frame bending under load might cause some of the load to be distributed to the pinned connection instead of the load cell. Third, the measurement of the location at which the force is applied to the load cell might be inaccurate because it is difficult to determine where the center of a distributed load lies. Finally, the measurement of the moment of inertia of the reaction wheel might be inaccurate due to the assumptions made during calculation such as the disk material being uniformally dense. These unaccounted factors may result in the consistent difference between the angular impulse calculated through load cell measurements and the angular impulse calculated through encoder measurements.

6 Future Work

Further work on this project would involve installing wheels on the car and controlling them using motors in conjunction with the reaction wheel. This would allow the car to drive around on the ground before reaching a stair and lifting itself up to climb onto the stair.

There are many parts of the control and design that need to be refined before this happens however. Most importantly, the safety aspects of the car pose a huge obstacle towards it being used for the desired application. A different containment system for the reaction wheel disk, perhaps installed on the car itself, would allow the car to move around outside a test cage without threatening the safety of bystanders. On the topic of the reaction

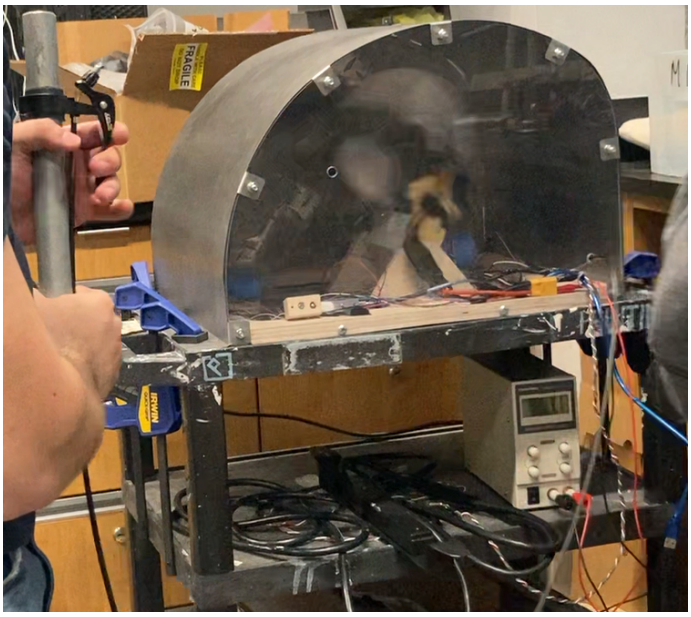

FIGURE 13. Car lifting motion due to brake impulse from hand actuation.

wheel disk, it is very large in its current state and will likely touch the corner of any stair it tries to climb. This feature will have to be drastically changed if it is to function as desired.

Another important point of development is the incorporation of automatic braking. Currently, the car uses a manually-actuated bike brake but that cannot be precisely controlled. In order to prevent generating too much or too little torque, it is necessary to install a method of controlling the braking force. If that is possible, the car could reach a rear wheel stand with minimal velocity. Once this is obtained, the car will require a PID loop on the reaction wheel motor so that it can stabilize the car in an inverted pendulum position. With full control over the car's braking and orientation, it will be possible to autonomously lift the car and traverse a stair.

A smaller point of improvement is revising material choices to minimize the weight of the car while maintaining structural strength. This can be done by using materials with a high strength-to-weight ratio such as carbon fiber as well as by minimizing mass in low-stress areas through the use of lightweight plastic. Additionally, the frame is extremely robust and overbuilt for its application. Future designs of the car should remove material and use more complex geometry to reduce weight while maintaining performance.

7 Appendix

7.1 Rotation Matrices

Rotation matrices are used when there are multiple reference frames in a system. When one frame is rotating with respect to another, rotation matrices can be used to relate a property expressed in one frame and express it in the other. Each frame will be expressed in terms of three orthonormal vectors which are the three axis. Because there are three axis in each frame, we can express each rotation as a rotation about one of these axes (or a combination of all three). For rotations about the one axis the rotation matrix is,

$$R^{(1)}(\psi) = \begin{bmatrix} 1 & 0 & 0 \\ 0 & \cos(\psi) & -\sin(\psi) \\ 0 & \sin(\psi) & \cos(\psi) \end{bmatrix} \tag{20}$$

The rotation matrices about the two and three axes are,

$$R^{(2)}(\psi) = \begin{bmatrix} \cos(\psi) & 0 & \sin\psi) \\ 0 & 1 & 0 \\ -\sin(\psi) & 0 & \cos\psi) \end{bmatrix} \tag{21}$$

$$R^{(3)}(\psi) = \begin{bmatrix} \cos(\psi) & -\sin(\psi) & 0 \\ \sin(\psi) & \cos(\psi) & 0 \\ 0 & 0 & 1 \end{bmatrix} \tag{22}$$

These rotation matrices are all clockwise right-handed rotations about each axes. To rotate the other way, one can either put in a negative angle or use the transpose of the rotation matrix (which in all three cases just flips the sign of the sine terms)

You can also multiply rotation matrices to rotate about multiple axes (Note that multiplying rotation matrices is not commutative, the order in which you rotate matters).

In practice, a rotation matrix can be used as follows. Suppose the zero frame, $E^{(0)}$. related to the one frame through a right hand rotation about the three axis by an angle θ and the two frame is related to the one frame by a counterclockwise rotation about the one axis by an angle ψ. To express the $E^{(0)}$ vector in the two frame we apply the appropriate rotation matrices. The superscript on the rotation matrix denotes which frame we are rotating from and which frame we are rotating to.

$$E^{(2)} = E^{(0)}\mathbf{R}^{(0,1)}\mathbf{R}^{(1,2)}$$

$$= E^{(0)} \begin{bmatrix} \cos(\theta) & -\sin(\theta) & 0 \\ \sin(\theta) & \cos(\theta) & 0 \\ 0 & 0 & 1 \end{bmatrix} \begin{bmatrix} 1 & 0 & 0 \\ 0 & \cos(\psi) & -\sin(\psi) \\ 0 & \sin(\psi) & \cos(\psi) \end{bmatrix}^T$$

7.2 Full Derivation of $\dot{H}$

$$H^{(3)}_{C,total} = \mathbf{E}^{(3)} J^{(3)}_c \boldsymbol{\omega}^{(3)} \tag{23}$$

In matrix form, this is equivalent to,

$$H^{(3)}_C = \begin{bmatrix} \mathbf{e}^{(3)}_1 & \mathbf{e}^{(3)}_2 & \mathbf{e}^{(3)}_3 \end{bmatrix} \begin{bmatrix} mr^2/4 & 0 & 0 \\ 0 & mr^2/4 & 0 \\ 0 & 0 & mr^2/2 \end{bmatrix} \begin{bmatrix} \dot{\theta} cos(\phi) \\ -\dot{\theta} sin(\phi) \\ \dot{\phi} \end{bmatrix}$$

Now, taking the derivative.

$$\dot{H}_c = \dot{\mathbf{E}}^{(3)} J^{(3)}_c \boldsymbol{\omega}^{(3)} + \mathbf{E}^{(3)} J^{(3)}_c \dot{\boldsymbol{\omega}}^{(3)}$$

Using the property that $\dot{\mathbf{E}}^{(3)} = \mathbf{E}^{(3)} \tilde{\omega}^{(3,3)}_{3/0}$, where,

$$\tilde{\omega}^{(3,3)}_{3/0} = \begin{pmatrix} 0 & -w^{(3)}_3 & w^{(3)}_2 \\ w^{(3)}_3 & 0 & -w^{(3)}_1 \\ -w^{(3)}_2 & w^{(3)}_1 & 0 \end{pmatrix} \tag{24}$$

,

$$\dot{H}_c = \mathbf{E}^{(3)} (\tilde{\omega}^{(3,3)}_3 J^{(3)}_c \boldsymbol{\omega}^{(3)} + J^{(3)}_c \dot{\boldsymbol{\omega}}^{(3)}) \tag{25}$$

The first term in the equation is,

$$\begin{bmatrix} 0 & -\dot{\phi} & -\dot{\theta} sin(\phi) \\ \dot{\phi} & 0 & -\dot{\theta} cos(\phi) \\ \dot{\theta} sin(\phi) & \dot{\theta} cos(\phi) & 0 \end{bmatrix} \begin{bmatrix} mr^2/4 & 0 & 0 \\ 0 & mr^2/4 & 0 \\ 0 & 0 & mr^2/2 \end{bmatrix} \begin{bmatrix} \dot{\theta} cos(\phi) \\ -\dot{\theta} sin(\phi) \\ \dot{\phi} \end{bmatrix}$$

$$= \begin{bmatrix} -J_2 \dot{\phi} \dot{\theta} \sin(\phi) \\ -J_2 \dot{\phi} \dot{\theta} \cos(\phi) \\ 0 \end{bmatrix} \tag{26}$$

Since $J_1 = J_2 = \frac{1}{2} J_2$.

The second term, where $\dot{\phi}$ and $\dot{\psi}$ are constant (no acceleration) is

$$\begin{bmatrix} mr^2/4 & 0 & 0 \\ 0 & mr^2/4 & 0 \\ 0 & 0 & mr^2/2 \end{bmatrix} \begin{bmatrix} -\dot{\theta} sin(\phi) \dot{\phi} \\ -\dot{\theta} cos(\phi) \dot{\phi} \\ 0 \end{bmatrix} = \begin{bmatrix} -J_2 \dot{\theta} sin(\phi) \dot{\phi} \\ -J_2 \dot{\theta} cos(\phi) \dot{\phi} \\ 0 \end{bmatrix} \tag{27}$$

Adding these two parts together yields,

$$\dot{H}^{(3)}_C = \mathbf{E}^{(3)} \begin{bmatrix} -J_3 \dot{\phi} \dot{\theta} \sin(\theta) \\ -J_3 \dot{\phi} \dot{\theta} \cos(\theta) \\ 0 \end{bmatrix} \tag{28}$$

Now we can perform appropriate rotation matrices on this to get the change in angular momentum in the one frame (car frame). The first rotation is around the third axis an angle ϕ to go from the three frame to the two frame. Since, $\mathbf{E}^{(2)} = \mathbf{E}^{(1)} \mathbf{R}^{(1,2)}$ we can write the equation as,

$$\dot{H}^{(2)}_C = \mathbf{E}^{(1)} \mathbf{R}^{(1,2)} \begin{bmatrix} -J_3 \dot{\phi} \dot{\theta} \sin(\theta) \\ -J_3 \dot{\phi} \dot{\theta} \cos(\theta) \\ 0 \end{bmatrix}$$

$$= \mathbf{E}^{(1)} \begin{bmatrix} \cos(\phi) & -\sin(\phi) & 0 \\ \sin(\phi) & \cos(\phi) & 0 \\ 0 & 0 & 1 \end{bmatrix} \begin{bmatrix} -J_3 \dot{\phi} \dot{\theta} \sin(\theta) \\ -J_3 \dot{\phi} \dot{\theta} \cos(\theta) \\ 0 \end{bmatrix}$$

$$= \begin{bmatrix} -J_3 \dot{\phi} \dot{\theta} \sin(\theta) \cos(\phi) \\ -J_3 \dot{\phi} \dot{\theta} \cos(\theta) \\ 0 \end{bmatrix}$$

References

[1] K. O. Austefjord, L.-K. S. Larsen, M. O. Hestvik, and T. J. Impelluso. Modelling subsea rov robotics using the moving frame method. International Journal of Dynamics and Control, 7:1306–1320, 2019.

[2] É. Cartan. On manifolds with an affine connection and the theory of general relativity, translated by a. Magnon and A. Ashtekar, Napoli, Italy, Bibiliopolis, 1986.

[3] M. E. Eia, E. M. Vigre, and T. R. Rykkje. Modeling a knuckle-boom crane control to reduce pendulum motion using the moving frame method. In ASME International Mechanical Engineering Congress and Exposition, volume 59414, page V004T05A069. American Society of Mechanical Engineers, 2019.

[4] K. Fischer. The shrinking of higher ed. https://www.chronicle.com/article/the-shrinking-of-higher-ed, 2022. Accessed: May 1, 2023.

[5] J. Flatlandsmo, T. Smith, Ø. O. Halvorsen, and T. J. Impelluso. Modeling stabilization of crane-induced ship motion with gyroscopic control using the moving frame method. Journal of Computational and Nonlinear Dynamics, 14(3), 2019.

[6] T. Frankel. The geometry of physics: an introduction. Cambridge university press, 2011.

[7] T. J. Impelluso. Assessing cognitive load theory to improve student learning for mechanical engineers. The Amer. Jrnl. of Distance Education, 23(4):179–193, 2009.

[8] H. B. Korsvik, E. S. Rognsvåg, T. H. Tomren, J. F. Nyland, and T. J. Impelluso. Dual gyroscope wave energy converter. In ASME International Mechanical Engineering Congress and Exposition, volume 59438, page V006T06A008. American Society of Mechanical Engineers, 2019.

[9] D. M. Luchtenburg, M. Shah, T. J. Impelluso, and T. Ravneberg Rykkje. A projection-based derivation of the equations of motion for the moving frame method for multi-body dynamics. In ASME International Mechanical Engineering Congress and Exposition, volume 85659, page V009T09A005. American Society of Mechanical Engineers, 2021.

[10] T. R. Rykkje, D. Leinebø, E. S. Bergaas, A. Skjelde, and T. J. Impelluso. Modeling friction in robotic systems using the moving frame method in dynamics. International Journal of Mechanical Engineering Education, 49(1):25–59, 2021.